Reconstructing air shower parameters with MGMR3D

P. Mitra,[1,2,*] O. Scholten[ORCID],[3,4,†] T. N. G. Trinh[ORCID],[5] S. Buitink,[2,6] J. Bhavani[ORCID],[7] A. Corstanje,[2,6] M. Desmet[ORCID],[2] H. Falcke,[6,8] B. M. Hare[ORCID],[3,4] J. R. Hörandel,[6,4] T. Huege,[9,2] N. Karastathis,[9] G. K. Krampah,[2] K. Mulrey,[6,4] A. Nelles,[10,11] H. Pandya,[2] S. Thoudam,[7] K. D. de Vries[ORCID],[4] and S. ter Veen[12]

[1]*University of Warsaw, Pasteura 5, 02-093 Warsaw, Poland*
[2]*Astrophysical Institute, Vrije Universiteit Brussel, Pleinlaan 2, 1050 Brussels, Belgium*
[3]*Kapteyn Institute, University of Groningen, Landleven 12, 9747 AD Groningen, The Netherlands*
[4]*Vrije Universiteit Brussel, Dienst ELEM, Brussels, Belgium, 1050 Brussels, Belgium*
[5]*Physics Education Department, School of Education, Can Tho University,*
Campus II, 3/2 Street, Ninh Kieu District, Can Tho City 94000, Vietnam
[6]*Department of Astrophysics/IMAPP, Radboud University Nijmegen,*
Heyendaalseweg 135, 6525 AJ Nijmegen, The Netherlands
[7]*Khalifa University, P.O. Box 127788, Abu Dhabi, United Arab Emirates*
[8]*Nikhef, Science Park 105, 1098 XG Amsterdam, The Netherlands*
[9]*Institut für Astroteilchenphysik, KIT, P.O. Box 3640, 76021, Karlsruhe, Germany*
[10]*Deutsches Elektronen-Synchrotron DESY, Platanenallee 6, 15738 Zeuthen, Germany*
[11]*Erlangen Center for Astroparticle Physics (ECAP), Friedrich-Alexander-Universität*
Erlangen-Nürnberg, Nikolaus-Fiebiger-Straße 2, 91058 Erlangen, Germany
[12]*Netherlands Institute for Radio Astronomy (ASTRON), Oude Hoogeveensedijk 4,*
7991 PD Dwingeloo, The Netherlands

Measuring the radio emission from cosmic-ray particle cascades has proven to be a very efficient method to determine their properties such as the mass composition. Efficient modeling of the radio emission from air showers is crucial in order to extract the cosmic-ray physics parameters from the measured radio emission. MGMR3D is a fast semianalytic code that calculates the complete radio footprint, i.e., intensity, polarization, and pulse shapes, for a parametrized shower-current density and can be used in a chi-square optimization to fit a given radio data. It is many orders of magnitude faster than its Monte Carlo counterparts. We provide a detailed comparative study of MGMR3D to Monte Carlo simulations, where, with improved parametrizations, the shower maximum X_{max} is found to have very strong agreement with a small dependency on the incoming zenith angle of the shower. Another interesting feature we observe with MGMR3D is sensitivity to the shape of the longitudinal profile in addition to X_{max}. This is achieved by probing the distinguishable radio footprint produced by a shower having a different longitudinal profile than usual. Furthermore, for the first time, we show the results of reconstructing shower parameters for Low-Frequency Array data using MGMR3D, and obtaining a X_{max} resolution of 22 g/cm^2 and energy resolution of 19%.

I. INTRODUCTION

When a high-energy cosmic particle impinges on the atmosphere of Earth, it creates an extensive air shower (EAS). The electrons and positrons in the plasma cloud at the shower front drift in opposite directions due to the Lorentz force caused by the geomagnetic field. Owing to this acceleration by an Earth's magnetic field and deceleration in interactions with air molecules a time varying transverse current is created. This varying current emits radio waves [1] where the intensity pattern on the ground, the intensity footprint, depends on the variation of the current with height. There is another subdominant contribution to the radiation from the excess of negative charge accumulated at the shower front, known as the "Askaryan effect" [2,3]. The penetration depth where the particle number reaches its maximum, X_{max}, strongly depends on the specifics of the first interaction, which strongly correlates with the mass of cosmic-ray primary. Different values of X_{max} result in differences in the longitudinal variation of the currents which is reflected in the intensity of the radio footprint. Thus X_{max} can be reconstructed on the basis of the footprint which allows for a determination of the mass composition of cosmic rays [4].

The modeling of radio emission from EAS is generally performed with either microscopic or macroscopic

[*]pmitra@fuw.edu.pl
[†]o.scholten@rug.nl

formalisms. In a microscopic formalism the emission is calculated for each particle as obtained from a Monte Carlo simulation of the EAS. The coherence of the signals emerges naturally in this approach. ZHAires [5] and CoREAS [6] are the two most commonly used microscopic codes.

MGMR [1], EVA [7,8], and their latest successor MGMR3D [9] are examples of macroscopic codes. In this framework, the radiation field is derived from the Liénard-Wiechert potential [10] where the four current is parametrized. The amplitude of the four current is explicitly split into the charge component driving the charge-excess emission and the transverse drift current generating the geomagnetic emission. One advantage of MGMR3D is that it is computationally inexpensive and produces radio profiles about 4 orders of magnitude faster than the Monte Carlo simulations. Another advantage is that it is fully deterministic in the sense that one can have control over the outputs by choosing exact shower parameters like the shower maximum and shape parameters of the longitudinal profile, contrary to the inherent randomness in Monte Carlo simulations. For these reasons, MGMR3D can be used to fit a reference radio footprint and obtain the corresponding longitudinal shower parameters that best reproduce the given profile through minimization techniques. There are other, more phenomenological approaches emerging like template synthesis [11] and radio morphing [12], that also allow a fast calculation of the radio footprint.

In MGMR3D the charge-current cloud of the air shower is parametrized which necessarily approximates its full complexity. In particular, the dependence on the energy of the particles forming this cloud is ignored; however, as the important particles in this cloud are relativistic, this is thought to be a reasonable approximation. In a prior publication [9], the parametrization and the foundation of the MGMR3D framework were introduced. In this follow-up work, we further investigate the performance of MGMR3D on ensembles of air showers and have refined the parametrization in an extensive comparative study with CoREAS. Most significantly, we have used MGMR3D to reanalyze measured data obtained with the Low-Frequency-Array (LOFAR) telescope. The MGMR3D-based analysis reproduces, within statistical significance, the results of an earlier analysis based on microscopic CoREAS calculations. MGMR3D offers thus a very CPU-efficient alternative to existing approaches for extracting shower parameters like X_{max} from the radio footprint, and thus composition, of the original cosmic rays. Notably, MGMR3D is also a strong tool to map atmospheric electric fields under thunderstorms. In a separate publication [13] a detailed study is presented of using MGMR3D for reconstructing atmospheric electric fields during thunderstorm conditions from the radio footprint of air showers.

This article is structured as follows. In Sec. II we describe the improved modeling of the radiation profile. In Secs. III and IV, comparisons between CoREAS with MGMR3D shower profiles are demonstrated, and the details of the results of fitting X_{max}. We also present a correction formula to obtain the correct zenith angle dependency for X_{max} as

compared to CoREAS calculations. Such a correction is necessary since the penetration depth for which the coherent transverse current is maximal generally differs from the penetration depth for which the number of charged particles is maximal, X_{max}. In Sec. V we show the results of reconstructing X_{max} using MGMR3D on measured LOFAR cosmic-ray data and compare to the existing X_{max} reconstructed with the LOFAR analysis method, as well as the reconstruction of shower core and energy.

II. MODELING RADIO EMISSION FROM EAS

The charge and current distributions that drive the radio emission from an EAS are expressed as a four current $j^\mu(t, x, y, h)$ where $\mu = 0$ denotes the time (charge) components, and $\mu = x$, y, z denote the space (current) components. The retarded Liénard-Wiechert potential for an observer at (t_o, x_o, y_o, z_o) in the shower plane with the retarded time t_r is

$$A^\mu(t_o, \vec{x_o}) = \int d^3\vec{x}' \frac{j^\mu(t_r, \vec{x}')}{\mathcal{D}}, \tag{1}$$

where the retarded distance is

$$\mathcal{D} = n\sqrt{(-\beta t_o + h)^2 + (1 - \beta^2 n^2)d^2}, \tag{2}$$

where the distance between the observer and the point of impact of the core of the air shower is denoted by d, and the index of refraction is denoted by n.

Since for a cosmic-ray air shower the particles are concentrated in a relatively flat pancakelike structure moving with relativistic speeds, the four current is parametrized as

$$j^\mu(t, x, y, h) = \frac{w(r)}{r} f(h, r) J^\mu(t). \tag{3}$$

The term $w(r)/r$ in Eq. (3) is the radial description of the plasma cloud, and the second term $f(h, r)$ is the current density of the shower front. These two are normalized such that $J^\mu(t)$ is the charge and current for a fixed time integrated over the complete plasma of the EAS. The radial dependence of the transverse current is parametrized as

$$w(r) = N_w \zeta(\zeta + 1)^{-2.5}, \tag{4}$$

with $\zeta = r/R_0$. The function $w(r) \times r$ corresponds to the Nishimura-Kamata-Greisen function [14] for a fixed shower age $s = 2$ [9]. These parametrizations were studied and optimized by comparing to the results of CONEX-MC [8]. The definition of R_0 is similar to the Molière radius, but not the same as in this context it is a scaling parameter that describes the radial current profile and thus is referred to as radiation radius. In the original formulation of MGMR3D the radiation radius was taken to be a constant. We observed that the optimum value for R_0 depends on the distance from X_{max} to the shower core ($D_{X_{max}}$), while fitting R_0 for different showers. We find that for distances smaller than 5 km R_0 is
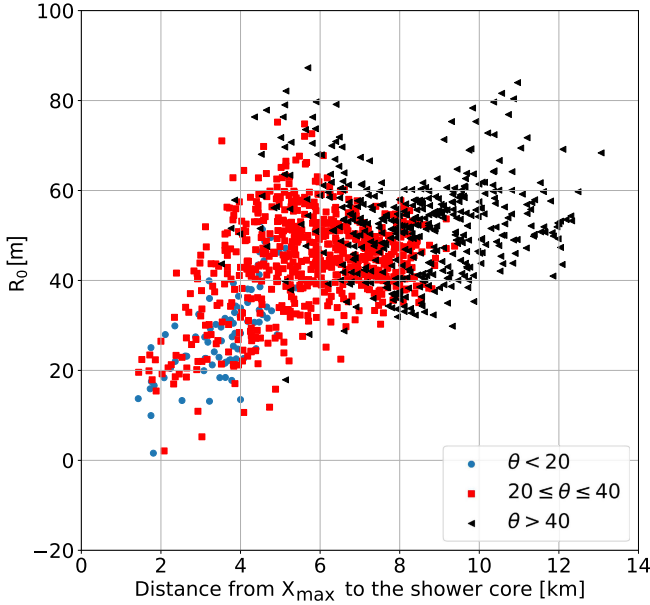
FIG. 1.   Radiation radius as a function of distance of X_{max} from shower core, obtained from comparing CoREAS showers to MGMR3D. Different colors show different zenith bands.

proportional to distance and reaches saturation with $R_0 = 50$ m for larger distances, independent of zenith angle. This is shown in Fig. 1. This linear dependency at smaller $D_{X_{max}}$ is now included in MGMR3D as $R_0 = 0.01D_{X_{max}}$.

The current density at a distance h behind the shower front is parametrized as

$$f(h, r) = N_f \frac{\eta}{e^{\sqrt{\eta}+1}}, \qquad (5)$$

where N_f is a normalization constant. The parameter λ, folded in as $\eta = h/\lambda$, accounts for the pancake thickness scaling and has a radial dependence. The radial dependence of the pancake thickness is described in a way that it is constant near the shower axis and increases linearly at distances away from the shower axis where particles tend to have less energy and thus lag behind. The parametrizations for the radial and pancake function were also studied and optimized with comparison to the results of CONEX-MC [8].

The functions w and f that depend on the distance to the shower axis are normalized according to $\int_0^\infty w(r)dr = 1$ and $\int_0^\infty f(h, r)dh = 1 \; \forall \; r$.

A. Parametrization of the currents

The original parametrization of the charge cloud in MGMR3D, as described in [9], was based on CONEX-MC simulations [8]. There were however important inconsistencies in the extracted shower parameters as well as in the observed radiation profile, when compared with the CoREAS results. A reason behind these differences is that in the parametrization the energy distribution of the particles in the shower is not taken into account. Parameters

like the drift velocity and charge excess are strongly dependent on the energy range of particles used to predict these averaged quantities. To mitigate these issues we revisit the parametrizations in this work by comparing the results of MGMR3D and CoREAS calculations for an ensemble of air showers. This leads to improved parametrizations, in particular for modeling the drift velocity (cf. Sec. II A) and for the longitudinal profile of the current, J^μ in Eq. (3). The details of the comparison between MGMR3D and CoREAS are presented in Sec. IV.

1. Transverse current

The transverse current is given by

$$\vec{J}_\perp(t_s) = N_c(X_z)\vec{u}_\perp(X_z), \qquad (6)$$

where the transverse drift velocity is denoted as $\vec{u}_\perp(X_z)$, and N_c is the number of charged particles at depth X_z. It should be noted that the penetration depth for X_{max} is only indirectly related to the penetration depth of the maximum transverse current, since the factor between the two, the drift velocity, depends on air density as well as the mean energy of the particles in the shower.

The drift velocity increases with increasing forces acting on the charges. This becomes particularly important for large electric fields in thunderstorm clouds, and special treatment is required so that the particles do not exceed the speed of light [15]. The transverse drift $\vec{u}_\perp(X_z)$ is therefore expressed as

$$\vec{u}_\perp(X_z) = \frac{c\vec{v}}{\sqrt{1 + v^2/v_0^2}}, \qquad (7)$$

where the parameter v_0 is adjusted to the value 0.2, and v is taken proportional to the Lorentz force.

In the original parametrization used in [9] no dependence on air density was assumed in the parametrization of the drift velocity. We noted that a $\sqrt{\rho}$ scaling was necessary to obtain agreement with the results of the CoREAS calculation. We thus updated the formula for the drift velocity to read as

$$\vec{v}(X_z) = \frac{c\vec{F}_\perp}{F_\beta} \times \frac{a_t + 1}{\frac{X_{max} - X_t}{X_z - X_t} + a_t} \times \sqrt{\frac{\rho(X_{max})}{\rho(X_z)}} \qquad (8)$$

with the friction constant $F_\beta = 250$ keV/c, $X_t = 50$ g/cm^2, and $a_t = 3$. The factor containing X_t and a_t determines the fractional magnitude of the drift velocity as compared to the value reached at X_{max}. This factor accounts for the fact that initially the shower particles move much slower under the influence of the Lorentz force. $\vec{F}_\perp$ is the total transverse force acting on the particles, and for the air showers when no thunderstorm is present it only consists of the Lorentz force, $\vec{F}_\perp = e\vec{v}_s \times \vec{B}$, where $\vec{v}_s$ is the velocity of the shower front, e is the elementary charge, and $\vec{B}$ is Earth's magnetic field. The second factor in Eq. (8) takes into account the fact that the drift velocity depends on the penetration depth in the

atmosphere, accounting for the changing mean energy of the shower particles. It is good to mention that this parametrization becomes less accurate for the highest zenith angles, where an additional dependence on emission height is seen. This correction is not yet included in the code, which should therefore be used with caution when studying highly inclined showers above 60° zenith angle. For the study reported in this article both simulated and recorded showers are well below this limit.

The physical interpretation of the $\sqrt{\rho}$ scaling is not trivial. Interestingly, the drift velocity has the same form as the terminal velocity due to the macroscopic drag force acting opposite to the relative motion of any object moving in a fluid. The drag force of air is proportional to the square of the speed of the object. For a falling object in air the terminal velocity can be reached when the force due to gravity balances the drag force

$$mg = F_D = \frac{1}{2}\rho C A v^2, \qquad (9)$$

with C, A, v being the drag coefficient, area of the object, and terminal velocity respectively. Solving for v results in

$$v = \sqrt{(2mg/\rho CA)}. \qquad (10)$$

The result can be generalized to situations where the object is accelerated by other forces. In the case of the electron drift velocity that would be the Lorentz force. The equivalent of the drag force is actually due to the many elastic collisions of the relativistic electron in the shower front with neutral air molecules. A relativistic electron in the shower lives roughly a microsecond (300 meters) before being stopped in a hard inelastic collision. Within that microsecond, the electron actually undergoes more than a million elastic collisions with particles in the air. While this provides an intuitive understanding of the $\rho^{-1/2}$ scaling, the assumption that an electron plasma experiences the same drag as a macroscopic object is of course not easily justified. It is worth mentioning that in [12] a similar density dependence on the electric field amplitude of radio pulse was reported in a study for the radio morphing method.

2. Charge excess

The charge excess in the shower is given as $J_Q(z) = eN_c(X_z)\rho_c(X_z)$ where e is the charge of the electron and the proportionality factor is $\rho_c(X_z)$ defined in the most recent form,

$$\rho_c(X_z) = J_Q^0 \frac{3X_z - X_{max} - X_c}{X_{max} + X_z - X_c}$$

$$\times \left(1 - e^{-\frac{X_z - X_c}{2(X_{max} - X_c)}}\right) \frac{\rho(X_{max})}{\rho_c} \sqrt{\frac{\rho(X_z)}{\rho_c}}, \qquad (11)$$

where J_Q^0 is a normalization constant, $\rho_c = 0.06$ g/cm³, and $X_c = 50$ g/cm². The first two factors in Eq. (11) are

inspired by comparing to the results of CONEX-MC simulations including simulations for highly inclined showers with zenith > 65°. The last term including the square root dependency on density is inspired from the treatment of the transverse current in Eq. (8).

B. Parametrization of the longitudinal profile

There are two common ways to parametrize the longitudinal profile, the number of charged particles at a depth X_z. One is the Gaisser-Hillas formula [16] for $N_c^{G-H}(X_z)$, and the other is the R, L formula in [17] for $N_c^{R-L}(X_z)$,

$$N_c^{G-H}(X_z) = N_{max} \times \left(\frac{X_z - X_0}{X_{max} - X_0}\right)^{\frac{X_{max} - X_0}{\Lambda}} e^{\frac{X_{max} - X_z}{\Lambda}} \qquad (12)$$

$$N_c^{R-L}(X_z) = N_{max} \times \left(1 - \frac{R}{L}(X_{max} - X_z)\right)^{R^{-2}} e^{\frac{X_{max} - X_z}{RL}}, \qquad (13)$$

where the number of particles at the shower maximum, N_{max} is taken proportional to the energy of the cosmic ray,

$$N_{max} = N_E^0 E_{cr}, \qquad (14)$$

where $N_E^0 = 10^{-5}$ is a normalization factor. The energy is one of the fit parameters in the MGMR3D calculation. The main difference between the two parametrizations is that the parameters in Eq. (12) are related to the physics of the shower such as the depth of the first interaction while R and L in Eq. (13) relate more directly to the rise and fall of the distribution [18]. These more general parametrizations provide the option to study effects of the longitudinal shape parameters other than X_{max} on the radio footprint [19]. In principle, either of these parametrizations can be used to describe the longitudinal profiles in MGMR3D. We have used Eq. (13) throughout this analysis.

The intensity of the radio pulse depends on the energy of the cosmic ray which is treated as a normalization factor, a proxy for the air shower energy, in MGMR3D when a χ^2 fit to data is performed. This normalization factor was introduced in Eq. (14). Thus, when fitting the radio footprint as generated by CoREAS simulations for showers with a fixed energy, the normalization factor should be constant, barring shower-to-shower fluctuations. In Fig. 2, we indeed show this is approximately constant, for showers at various zenith angles.

III. STOKES PARAMETERS AS OBSERVABLES

We investigate the radio footprint of an air shower using Stokes parameters since these capture the complete polarization structure of the radio pulse. Because the objective of the present work is to develop a scheme for data interpretation, we construct the Stokes parameters specific for the LOFAR frequency band, between a 30 and 80 MHz band.

The Stokes parameters can be expressed in terms of the complex observable $\mathcal{E}_i = E_i + i\hat{E}_i$, where E_i is the electric field component in the $\hat{e}_{\mathbf{v} \times \mathbf{B}}$ and $\hat{e}_{\mathbf{v} \times (\mathbf{v} \times \mathbf{B})}$ directions which
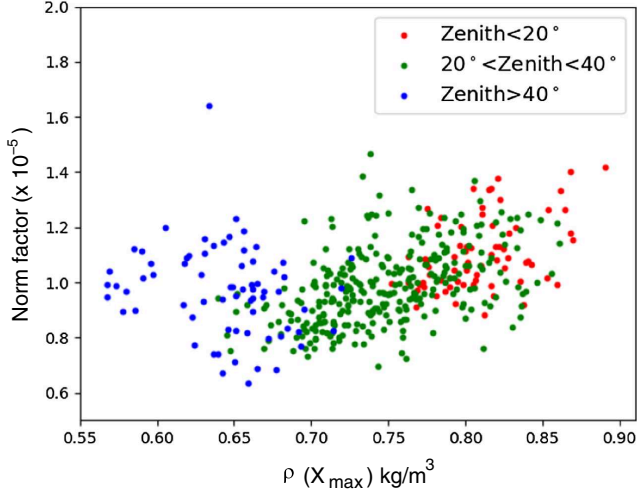
FIG. 2. Normalization factor as a function of the density at $X_{\max}$, obtained from MGMR3D by comparing to CoREAS showers. Different colors show different zenith angle bands.

are by construction perpendicular to the propagation direction of the shower, and $\hat{E}_i$ is its Hilbert transformation [20] (in arbitrary units), as

$$I = \frac{1}{N} \sum_0^{n-1} (|\mathcal{E}|^2_{i,\mathbf{v}\times\mathbf{B}} + |\mathcal{E}|^2_{i,\mathbf{v}\times(\mathbf{v}\times\mathbf{B})})$$

$$Q = \frac{1}{N} \sum_0^{n-1} (|\mathcal{E}|^2_{i,\mathbf{v}\times\mathbf{B}} - |\mathcal{E}|^2_{i,\mathbf{v}\times(\mathbf{v}\times\mathbf{B})})$$

$$U + iV = \frac{2}{N} \sum_0^{n-1} (\mathcal{E}_{i,\mathbf{v}\times\mathbf{B}}\mathcal{E}^*_{i,\mathbf{v}\times(\mathbf{v}\times\mathbf{B})}). \qquad (15)$$

We sum over the entire signal trace while calculating the values from CoREAS simulations. The linear-polarization angle with the $\mathbf{v} \times \mathbf{B}$ axis, ψ, can be calculated directly from the Stokes parameters as $\psi = \frac{1}{2}\tan^{-1}(U/Q)$. The relative amount of circular polarization is given by V/I, and it can be interpreted due to a time lag between the peak of the charge excess and transverse current pulses [21].

A. Noise-error estimate on Stokes parameters

MGMR3D performs a fit of the input radio profile through a Levenberg-Marquardt minimization procedure [22], that is based on a steepest descent method. The reduced χ^2 of the fit is defined as

$$\chi^2 = \frac{1}{N_{\mathrm{ndf}}} \sum_{a,f} \frac{(f_c^a - f_m^a)^2}{\sigma_{f^a}^2}, \qquad (16)$$

where f_c^a, and f_m^a are the different Stokes parameters calculated with CoREAS and MGMR3D respectively for antenna a, N_{ndf} is the number of degrees of freedom, and σ_f^a is the error on the Stokes parameter.

It is important to note that when we are performing a model-to-model comparison here, the numerator in Eq. (16)

TABLE I. List of fixed parameters in MGMR3D. OBSDIST_DIM is the grid dimension used for the calculation of antenna distance to the shower axis, J_{0Q} is the charge-excess normalization factor, and σ_n is the noise level. R and L are the shape parameters of the longitudinal profile fixed to their central values.

OBSDIST_DIM (m)	70
J_{0Q}	0.22
σ_n (J/m^2)	0.08
R	0.3
L (g/cm^2)	220

does not have a noise contribution, and the χ^2 can be $\ll 1$. For the sake of clarity we refer to this as $\tilde{\chi}^2$ throughout this paper to distinguish it from the standard χ^2.

In the present calculations, we calculated σ_f^a for the comparison with CoREAS as

$$\sigma_f^a = \frac{\Delta t}{2}\left(c\epsilon\frac{2}{N}\sigma_n I + \frac{2}{N}\sigma_n^2\right), \qquad (17)$$

where N is the length of the trace and σ_n is the noise fluence per sample; c, ϵ are the natural constants—velocity of light and permittivity of air in S.I. units; and Δt is the width of the time bins. In this formulation, various Stokes parameters have equal error bars because they are derived either from addition or subtraction of intensities in different polarization direction.

For measured cosmic-ray data the value of the noise level σ_n is obtained from measuring a time window of the recorded signal trace where no significant signal is present. In the case of MGMR3D, the value is chosen such that it is a close representation of the measurement. The value is shown in Table I.

IV. COMPARISON TO COREAS SIMULATIONS

With the improved parmetrizations of the current profile as given in Sec. II A we validate the performance of MGMR3D by fitting the radio footprint of showers simulated with CoREAS to that of MGMR3D. There is a range of parameters available in the framework of MGMR3D that can be tuned to achieve a good fit. We follow the approach where generic shower parameters, based on shower generality, are taken fixed, such as those given in Table I, while others, in particular those describing the longitudinal profile of the shower ($X_{\max}$, the shower maximum, and E, the shower energy) are fitted for each shower.

CoREAS simulations are performed on a star-shaped layout of antennas with the center on the shower axis and eight arms. Each arm contains 20 antennas, with a spacing of 25 m in the shower plane. The radio pulses are filtered between 30 and 80 MHz.

The results of each CoREAS simulation for the intensity I for all antennas of the grid are fitted with MGMR3D using a steepest descent algorithm treating $X_{\max}$ and E as free parameters. In these calculations, the core position is kept fixed to
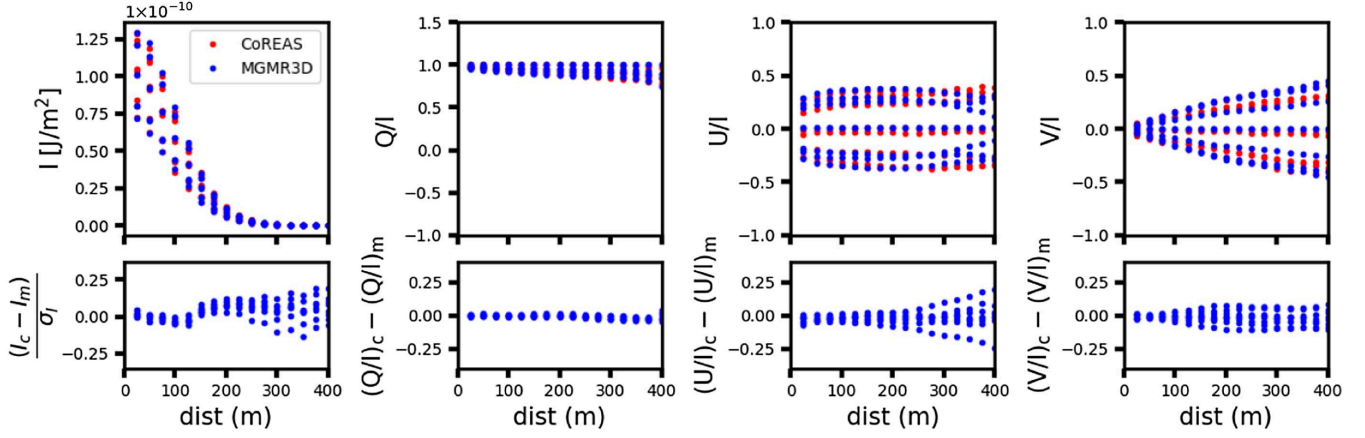
FIG. 3. Comparing Stokes parameters between best fitting MGMR3D and CoREAS, for a $10^{8.1}$ GeV shower with zenith angle $= 26°$ and $X_{\max} = 631$ g/cm^2. The top panel in each plot shows the Stokes parameter as a function of antenna distance, and the bottom panel shows the difference between CoREAS and MGMR3D. At each radial distance, there are eight data points corresponding to the antennas lying on different arms of the star-shaped layout.

the center of the grid. In later applications to LOFAR data (Sec. V) the core position is also treated as a free parameter.

A. Single shower comparisons

The different panels in Figs. 3 and 4 show the Stokes parameters for two showers coming in at a 26° and 46° zenith respectively. The top panels show the Stokes parameter as a function of antenna position for both MGMR3D and CoREAS, and the bottom panels show the relative difference between the two models defined as $\Delta I = \frac{(I_c - I_m)}{\sigma_I}$. The realistic error model described in Eq. (17) is used. All the plots show a common feature that the magnitude of ΔI varies with antenna positions and has zero crossings.

The magnitudes of the Stokes parameters depend on the azimuthal orientations of the antennas with respect to the core. For example, along the $\mathbf{v} \times \mathbf{B}$ direction there is full linear polarization resulting in $Q/I = 1$. It deviates from

unity for other directions, due to a small contribution from the charge-excess emission. Similarly, the circular polarization, expressed by V/I, is small and azimuth angle dependent.

The Stokes parameters U and V for the two calculations are shown to agree well within 250 meters, while the differences increase at larger distances. These differences seem to point to an underestimation of the difference in emission heights between charge excess and transverse current radiation in MGMR3D.

Figure 5 shows an example of a shower with a very large $X_{\max} \approx 950$ g/cm^2 which results in a poor agreement between CoREAS and MGMR3D; such cases can be expected when the shower develops close to the ground. Further details for such cases are discussed in Sec. IV B.

In the rest of this work, we concentrate on reconstructing the shower maximum using Stokes I. We restrict ourselves to I as it is the Stokes parameter that can most accurately be measured experimentally, and we have also noted that adding
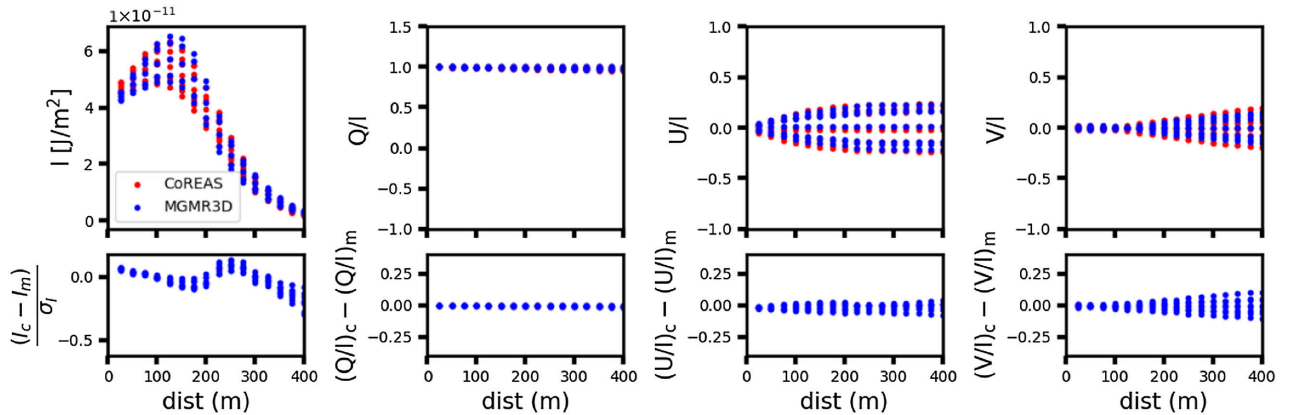

FIG. 4. Comparing Stokes parameters between best fitting MGMR3D and CoREAS, for a $10^{8.2}$ GeV shower with zenith angle $= 46°$ and zenith with $X_{\max} = 630$ g/cm^2. The top panel in each plot shows the Stokes parameter as a function of antenna distance, and the bottom panel shows the difference between CoREAS and MGMR3D. At each radial distance, there are eight data points corresponding to the antennas lying on different arms of the star-shaped layout.
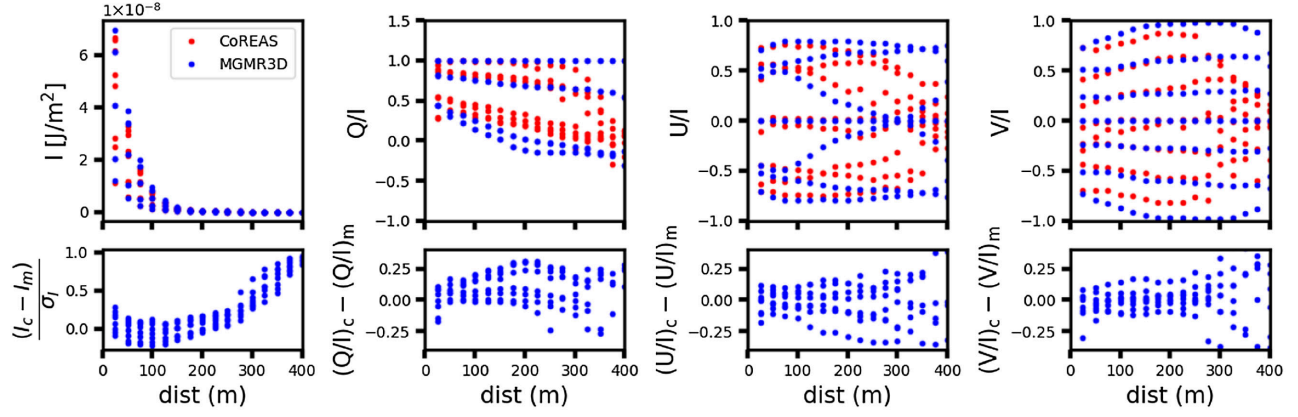
FIG. 5. Comparing Stokes parameters between best fitting MGMR3D to CoREAS, for a shower with very high $X_{max} = 940$ g/cm^2 with zenith angle $= 10°$ and shower energy $\approx 10^9$ GeV, where the fit quality is poor.

other Stokes parameters does not lead to any significant improvement in the reconstruction of air shower parameters. This, at first sight a surprising result, can be understood from the fact that in the absence of charge-excess emission one would expect a zero value for the U and V Stokes parameters. Their finite values are due to interference with the emission due to charge excess in the shower. Since the charge-excess fraction in the shower is kept fixed in the present analysis, the inclusion of the polarization-sensitive Stokes parameters in the analysis will not give a significant modification of the results.

B. Fitting the shower maximum

In this section, we report the results of reconstructing X_{max} with MGMR3D by fitting an ensemble of CoREAS showers. This CoREAS library was produced for each detected shower in LOFAR, where at least 25 proton and 10 iron showers are simulated with the same energy and arrival direction obtained from a preliminary reconstruction for this shower [23].

The radio footprints with MGMR3D are fitted to CoREAS with X_{max} as a free parameter for each shower with arrival direction and energy the same as CoREAS. As mentioned earlier, for CoREAS simulations the shower core positions are known; hence we do not fit the core positions. But for real data core positions become important fit parameters while obtaining the radio profile that best describes the data. This is discussed in detail in the next section.

We refer to the X_{max} values obtained from CORSIKA as X_{max}^{true} and the reconstructed values as X_{max}^{fit}. The results are shown in Fig. 6. This considers mixed primaries with proton and iron for various showers. The error calculated for the realistic noise model given in Eq. (17) is used. We have applied a quality cut based on the distance to X_{max} from the ground. Details of this cut are explained in the following paragraphs. The black crosses are the points that are excluded by the cut. A straight line is fit through the selected points, shown by the blue points. It is evident that there is a very strong correlation between the reconstructed X_{max} and the CoREAS truth values. The slope and intercepts of the fit are

0.98 and 19 respectively. Distribution of the deviation of X_{max}^{fit} from the fitting line, denoted by $\Delta X'$ is shown in the inset histogram of Fig. 6. This shows a resolution of 9.76 g/cm^2. It is also worth mentioning that we have studied the fits on proton and iron showers separately and found no bias on primary particle type. The fit results are found to be almost identical; we have thus used combined showers for the rest of the analysis.
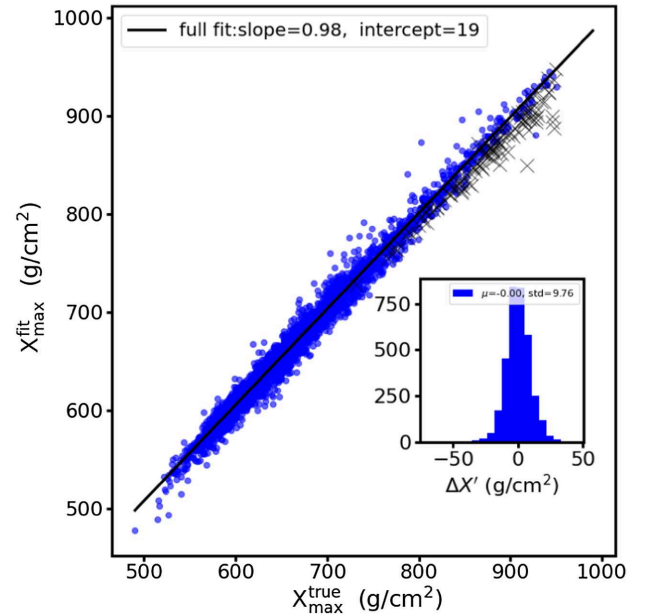

FIG. 6. Scatter plot of reconstructed X_{max} with MGMR3D and CoREAS. The ensemble contains showers with different energy, zenith, and azimuth angles, and for each shower at least 25 proton and 10 iron simulations are considered. A quality cut based on the distance from the core of the shower on the ground to X_{max} is applied. The black crosses represent showers excluded by the cut. The straight line is the best fitting line to the selected points passing the cut (blue). Distribution of the deviation of X_{max}^{fit} from the fitting line, denoted by $\Delta X'$ is shown in the inset histogram. The resolution of the fit is 9.76 g/cm^2.
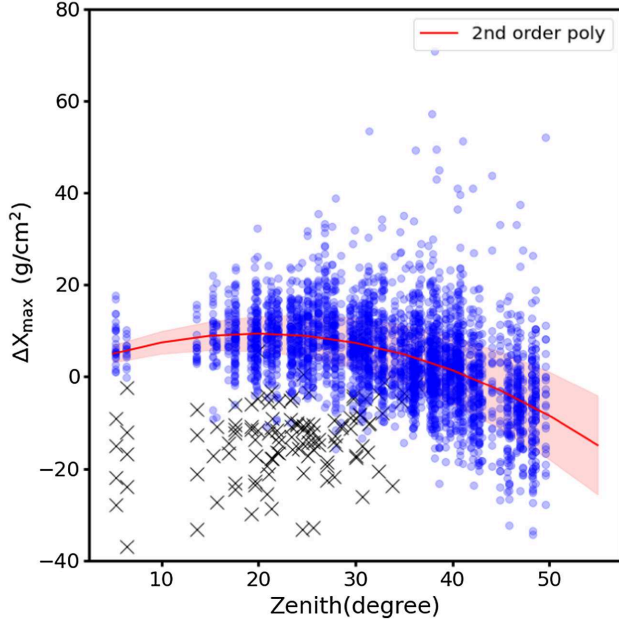
FIG. 7. Zenith angle distribution of ΔX_{max} of the showers shown in Fig. 6. The black crosses are showers having distance to X_{max} lower than 3 km and are excluded from the fit. The red line is a 2nd degree polynomial fit to the showers with the dashed line showing the 1-σ deviation. The fit coefficients are shown in Table II.

The shift in X_{max} from the true value is defined as $\Delta X_{max} = X_{max}^{fit} - X_{max}^{true}$. For the majority of the showers, ΔX_{max} is independent of X_{max} to the first order, as suggested by the near unity slope.

However, we have found a dependence on the shower zenith angle, as shown in Fig. 7, which includes the same showers as in Fig. 6. We see from the plot that there is a handful of outliers, a few in the positive direction of ΔX_{max} and more in the negative direction. The positive ones will be discussed in the next section. The negative outliers appear to be from showers that are developed closer to the ground. In order to obtain a clean parametrization to capture the relationship between ΔX_{max} and zenith, we have used a cut on the outliers. These outliers are excluded based on a cut on the distance from the core of the shower on the ground to X_{max}. We have chosen a conservative cut to accept showers with distance to $X_{max} > 3$ km in the fit that captures the trend between ΔX_{max} with respect to the zenith, shown by the red curve. The excluded points are shown in black crosses. For showers that are developed closer to the observer there are systematic differences between MGMR3D and CoREAS (also shown in a radio Lateral Distribution Function (LDF) example in Fig. 5), which could be attributed to the fact that for such showers more detailed parameters, like the dependence on the distance to the shower axis of the thickness and shape of the shower front, start to become important for the radio footprint, leaving room for more fine-tuning for specific showers with MGMR3D. Another important point is that, the general emission mechanism in MGMR3D

TABLE II. Polynomial fit of the form $\Delta X_{max} = p_0\, \theta^2 + p_1\, \theta + p_2$, where θ is the zenith of the shower in degrees and ΔX_{max} is the difference in X_{max} fitted with MGMR3D from the CoREAS truth value.

p_0	p_1	p_2
-1.94×10^{-1}	0.769	1.56

involving coherence and farfield assumptions start to become less accurate when the emission is generated close to the antennas. However, for the majority of the showers the generic approximations hold, and results with MGMR3D are in good agreement with COREAS.

The coefficients of the fit from Fig. 7 are given in Table II. This parametrization can be used as a correction factor to estimate the expected X_{max} value from X_{max}^{fit} in general and is used while fitting LOFAR data to MGMR3D in Sec. V.
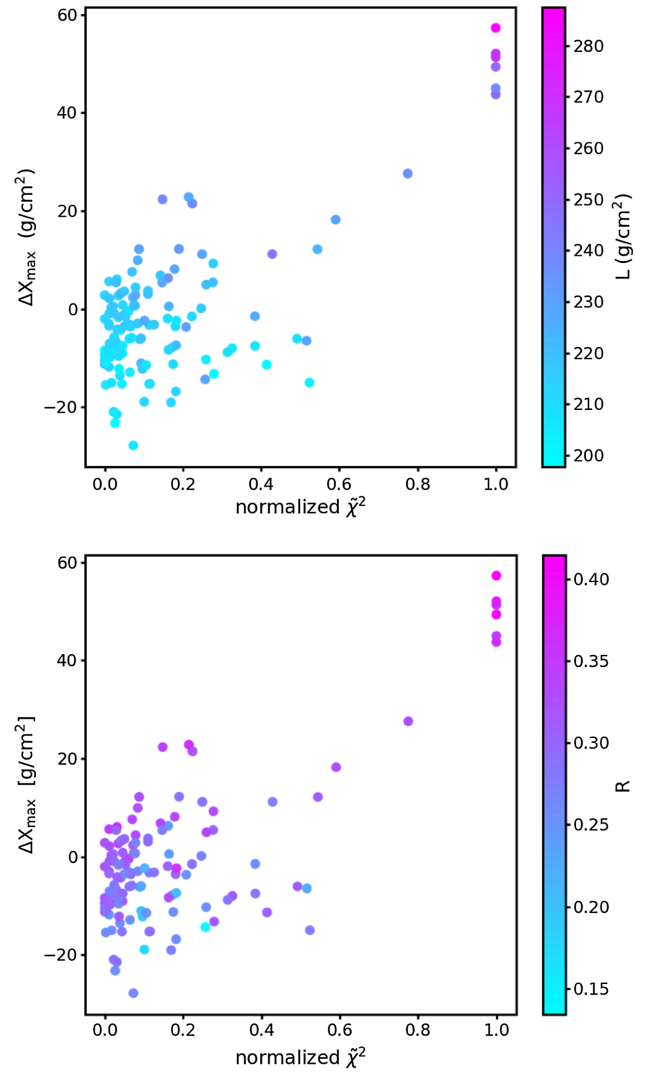

FIG. 8. ΔX_{max} as function of $\tilde{\chi}^2$ with color bars indicating true L (top) and R values (bottom) for an ensemble of proton simulations for a subset of showers. The $\tilde{\chi}^2$ values are normalized to 1 individually for each set of simulated showers.

C. Sensitivity to shower shape parameters—R and L

It appears from Fig. 7 that there are a few showers, where the X_{max} fit from MGMR3D is overestimated significantly from their CoREAS truth values that are not affected by the distance to the X_{max} cut described in the previous section. In this section, we take a closer look at some of these cases.

It was found that these outliers have significantly larger $\tilde{\chi}^2$ values than the other CoREAS simulations for the same shower angle and energy. We have ruled out the possibility of nonconvergence of the fit, by studying the $\tilde{\chi}^2$ surface for X_{max}, which showed a clear global minimum for all cases. While probing other reasons for such differences, we have found that these showers have longitudinal profiles that differ considerably from the rest of the ensemble. These differences are observed in terms of the shape parameters R and L as described in Eq. (13). It appears that for these outliers the true R and L values, obtained from fitting the CORSIKA longitudinal profiles are significantly higher than compared with their central values. Few of these outliers, along with their companion showers with the same energy, direction, etc., are shown in Fig. 8. Their true values of R and L are color coded. The $\tilde{\chi}^2$ values are normalized to 1 individually for each set of simulated showers. This way, the outliers are the showers with normalized $\tilde{\chi}^2 = 1$ and high ΔX_{max}, that have extreme R and L values.

The CORSIKA longitudinal profile for an extreme case is shown in Fig. 9. The shower shape is wider than usual, and this could indicate the presence of an energetic secondary shower.

In MGMR3D the R and L parameters are fixed to central values (see Table I), and we fit X_{max} only. This can explain the large shift in predicted X_{max} which arises to compensate for the difference in longitudinal profile; however, the $\tilde{\chi}^2$ for

these outliers still remains higher than the ensemble. This example clearly shows two important results. Firstly, the radio profiles are influenced by other parameters of the longitudinal profile than only X_{max}. Secondly, MGMR3D is sensitive to these parameters. To extract all three parameters, R, L, and X_{max}, from the MGMR3D calculation requires more dedicated efforts and currently is beyond the scope of this paper. However, the outliers are only a small fraction of the total number of showers, and this would have only a small effect on the zenith based correction proposed in Table II.

V. APPLICATION TO LOFAR DATA

In this section we discuss various steps of applying MGMR3D to experimental data and estimate X_{max}. We have used LOFAR cosmic-ray data for this purpose. Currently, LOFAR provides the highest precision for the determination of X_{max} with the radio technique [24]. The dense core of LOFAR consists of 288 low-band dipole antennas within an area with a diameter of 320 meters, known as the Superterp. The radio emission from air showers in the frequency range 30–80 MHz is recorded by the LOFAR low-band antennas [25]. An array of particle detectors, LORA, installed on the Superterp provides the trigger for the detection of the air showers [26].

The usual X_{max} reconstruction technique used at LOFAR is based on the production of dedicated CoREAS simulation sets for each detected air shower. The number of simulations needed to reconstruct the shower maximum is optimized with CONEX [27]. A set of CORSIKA simulations with proton and iron primaries is produced for each detected cosmic ray. The radio emission is simulated in a star-shaped pattern for antenna positions in the shower plane using CoREAS. For each CoREAS simulation the value of X_{max} as well as the χ^2 is determined when fitting the core position to data. X_{max} for a measured shower is then reconstructed by fitting a parabola to the χ^2 vs Monte Carlo X_{max} contour. The latest results on LOFAR cosmic-ray analysis can be found in [28]. While such a Monte Carlo based approach is precise, it is compute intensive. Thus, fast alternatives such as MGMR3D are desired, where X_{max} is reconstructed in the steepest descent optimization of the parametrized radio profile to given data.

The details of applying MGMR3D to data are as follows. The quantity P_{data} or P_{mgmr3d}, is calculated as the time integrated voltage squared over a 55 ns window centered around the pulse maximum, and is used as the observable. The error, σ_P, is estimated from the measurement of the noise level from data. This is the same procedure as used in [28]. This implementation is different from the previous case of fitting only to simulations where the Stokes parameters, integrated over the full trace, were used as observables.

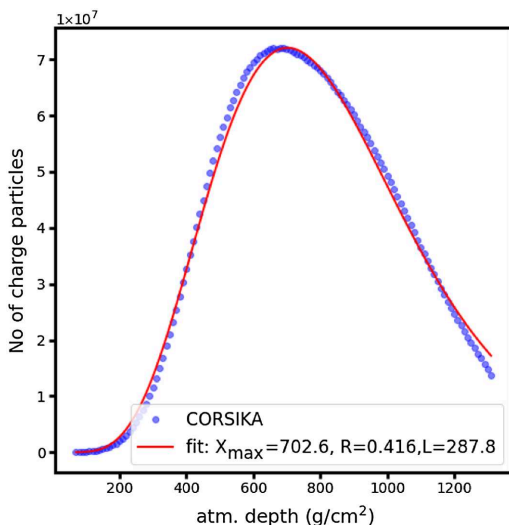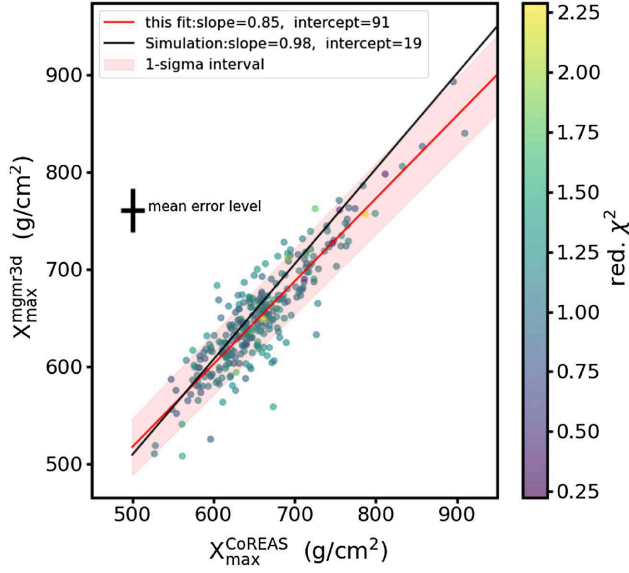The reduced χ^2 to be minimized in MGMR3D is defined as

FIG. 9. Longitudinal profile for a simulated shower. This is one of the extreme cases shown in Fig. 8 that has normalized $\tilde{\chi}^2 = 1$. The dots are the CORSIKA values, and the line is fit to the profile.

FIG. 10. Reconstructed X_{max} with MGMR3D and LOFAR. The X_{max} values reconstructed with MGMR3D are corrected with the zenith correction from Table II. The mean error bar is shown by the black cross. The red line is the fit to the data points considering the vertical mean error in the fit. The shaded area is the 1-σ interval of the fit. The black line corresponds to the prediction from simulation as discussed in Sec. IV B.

$$\chi^2 = \frac{1}{N} \sum_{\mathrm{antennas}} \left(\frac{P_{\mathrm{data}} - P_{\mathrm{mgmr3d}}(x_{\mathrm{core}}, y_{\mathrm{core}}, X_{\mathrm{max}})}{\sigma_P} \right)^2, \quad (18)$$

where X_{max} and the core positions $(x_{\mathrm{core}}, y_{\mathrm{core}})$ are the free parameters of the fit. The shower energy for the MGMR3D
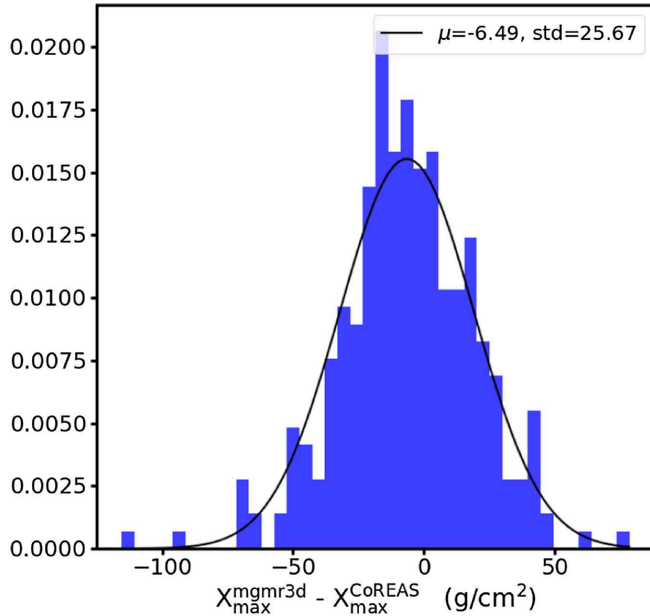

FIG. 11. The distribution of $X_{\mathrm{max}}^{\mathrm{mgmr3d}} - X_{\mathrm{max}}^{\mathrm{CoREAS}}$ is fitted by a Gaussian with $\mu = -6.49\,\mathrm{g/cm}^2$ and a standard deviation $\sigma_{\mathrm{tot}} = 25.67\,\mathrm{g/cm}^2$.

calculation is determined from the normalization constant; see Eq. (14).

In fitting to the data we have kept the longitudinal shape parameters R and L as well as the charge-excess parameter J_{0Q} fixed to the values given in Table I. Including these parameters in the fit sometimes gave rise to a poor convergence without considerably improving the fit quality.

The core reconstruction from a parametrization of the radio LDF [29] is used as initial guesses for the core positions, the same as was also used in the CoREAS reconstruction method. In order to fit X_{max}, it is seen that starting from a small value between 300 and 400 $\mathrm{g/cm}^2$ leads to faster convergence.
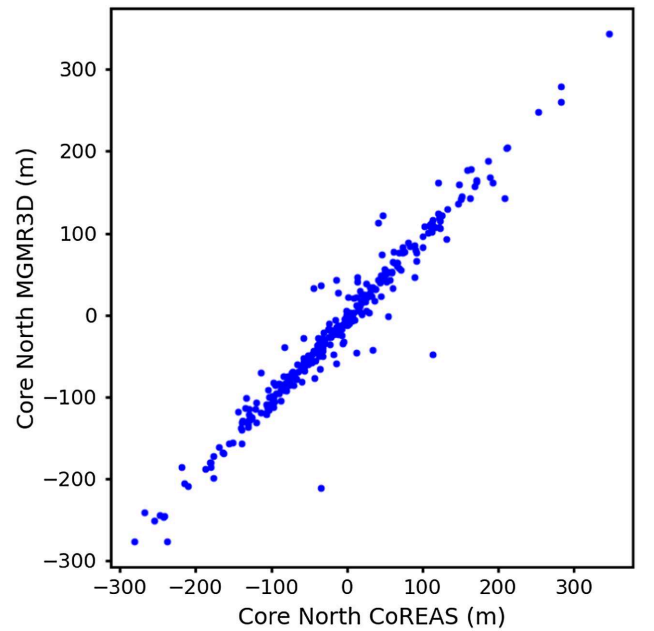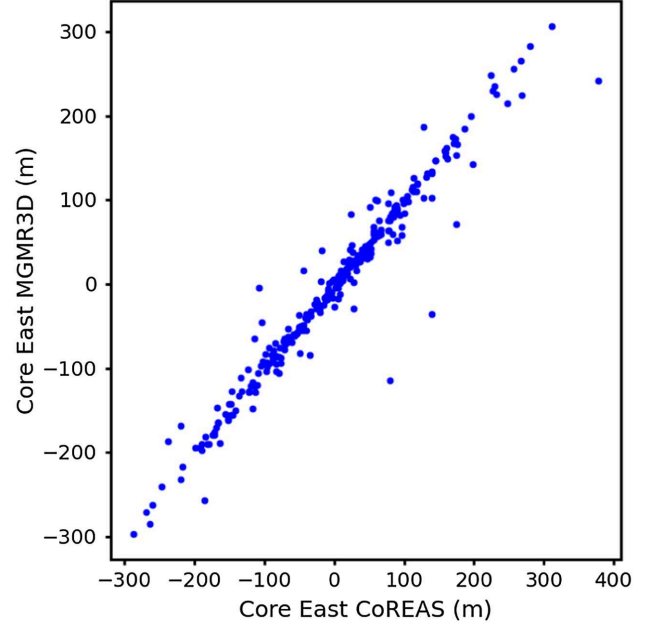

FIG. 12. Correlation in reconstructed cores for all showers between CoREAS and MGMR3D for two directions.

The reconstructed X_{max} with MGMR3D are shown in comparison to the obtained X_{max} using the LOFAR reconstruction technique in Fig. 10. The X_{max} values reconstructed with MGMR3D are corrected with the zenith correction formula described in Table II. We have also implemented the distance to the X_{max} based quality cut as described in Sec. IV B. The red line is a linear fit to the data with a slope of 0.85 and intercept of 91. The shaded area is the 1-σ error on the fit. The black line is the prediction from simulations only, as discussed (cf. Fig. 6).

From the comparison shown in Fig. 10 an estimate can be obtained for the accuracy for $X_{\mathrm{max}}^{\mathrm{mgmr3d}}$. The combined error on X_{max} is calculated from the standard deviation of the Gaussian fitted to the distribution of $X_{\mathrm{max}}^{\mathrm{mgmr3d}}$—$X_{\mathrm{max}}^{\mathrm{CoREAS}}$ as shown in Fig. 11. Assuming the errors due to MGMR3D and CoREAS reconstruction are uncorrelated the total error σ_{tot} can be written as

$$\sigma_{\mathrm{tot}}^2 = \sigma_{\mathrm{coreas}}^2 + \sigma_{\mathrm{mgmr3d}}^2, \tag{19}$$

where σ_{coreas} is obtained from the mean of the distribution of errors on X_{max} reconstructed with CoREAS for individual events, using a Monte Carlo method [24]. With $\sigma_{\mathrm{coreas}} = 14.5 \ \mathrm{g/cm^2}$ we obtain $\sigma_{\mathrm{mgmr3d}} = 21.2 \ \mathrm{g/cm^2}$. This value is used as the resolution of the X_{max} reconstruction with MGMR3D from LOFAR data and shown in the black cross in Fig. 10. Since for CoREAS the shower is given by a microscopic CORSIKA calculation, it is possible to obtain the error on X_{max} from the quality of the fit, but for MGMR3D such a procedure is not possible. The reason is that in MGMR3D calculations, parameters entering in the longitudinal profile, can easily vary well outside the physical regime.

An example of the radio profile of a reconstructed shower is shown in Appendix A for both CoREAS and MGMR3D.

A. Reconstruction of shower core and energy

In Fig. 12 we show the correlation between the core positions reconstructed using MGMR3D and CoREAS reconstructed core positions. For the majority of the showers, the core positions show good agreement between COREAS and MGMR3D reconstructions. However, there are a few exceptions with large deviations between MGMR3D and CoREAS. This effect is not found to be correlated either with ΔX_{max} or χ^2. Some of these events are hard to reconstruct because the signal-to-noise ratio is relatively low, while others have a core that it is not well contained by the LOFAR stations. In both cases, small differences between CoREAS and MGMR3D can have an impact that is larger than usual.

In Fig. 13 the differences in cosmic-ray energy reconstruction between MGMR3D, using Eq. (14), and CoREAS are compared. The top panel of Fig. 13 shows that there is no clear correlation between the two. The bottom panel of the figure shows the relative difference, defined as
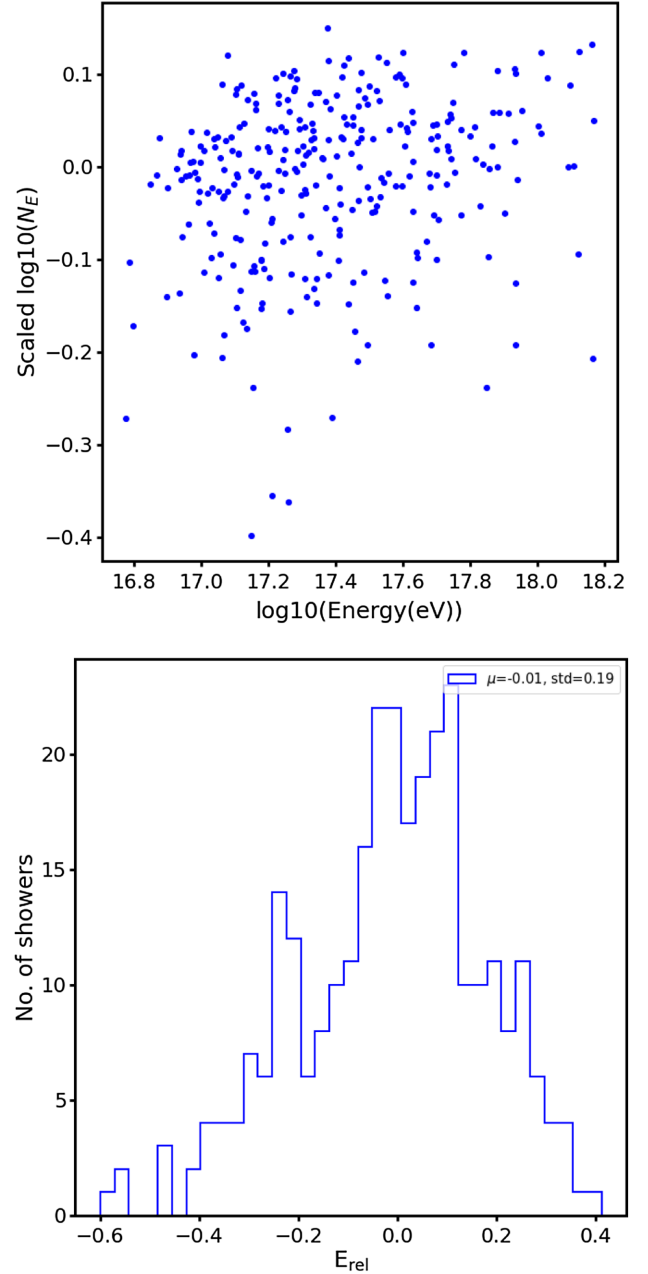

FIG. 13.   Top: the energy ratio $N_E = E_{\mathrm{mgmr3d}}/E_{\mathrm{CoREAS}}$ from the MGMR3D and CoREAS reconstructions of LOFAR data as a function of the CoREAS values, E_{CoREAS}. Bottom: the distribution of relative energy defined in Eq. (20).

$$E_{\mathrm{rel}} = 2 \frac{(E_{\mathrm{mgmr3d}} - E_{\mathrm{CoREAS}})}{(E_{\mathrm{mgmr3d}} + E_{\mathrm{CoREAS}})} \tag{20}$$

to make the differences more quantitative. This shows that there is no average offset between the two energy reconstructions. The spread of 19% in the distribution is comparable to the LOFAR energy resolution of 14% [30].

VI. SUMMARY AND CONCLUSIONS

The MGMR3D code, which uses an analytic parametrization of the plasma cloud, provides a promising alternative

to obtain the longitudinal structure of an air shower that best reproduces the measured radio footprint through minimization. It is computationally orders of magnitude faster than its microscopic counterparts that are customarily used for analyzing radio emission from cosmic rays. We have reported on a detailed comparison for a large ensemble of showers simulated with CoREAS and MGMR3D. This resulted in an optimized parametrization inside MGMR3D, in particular concerning the drift velocity, the charge excess, and the radial structure. With the optimized parametrization a strong agreement with microscopic CoREAS simulations was obtained for the lateral distribution functions for radio emission with a relative difference in intensity up to 10%.

As a follow-up step we have shown that MGMR3D can be used in a chi-square fit procedure to extract the shower maximum X_{max} for a large ensemble of showers simulated by CoREAS. The results show a very good agreement with a small systematic zenith-angle dependency, which is up to 6–8 g/cm^2 for zenith angles not exceeding 50 degrees. We introduce a correction formula to compensate for this. However, MGMR3D is not yet fully optimized for highly inclined showers with a zenith above 65 degrees. This is a prospect for a future effort and would be useful for simulation studies for experiments such as the Giant Radio Array for Neutrino Detection designed for detecting highly inclined air showers.

We have also found that MGMR3D is sensitive to the effects of additional parameters corresponding to the shape of the longitudinal shower profile on the radio footprint— namely R and L. These parameters have the potential to provide further insight in mass composition, constraining the hadronic model, as well as the astrophysical interpretation of cosmic-ray sources, in addition to X_{max} [31]. Probing these subtle parameter spaces requires extremely dense antenna layouts such as the Square Kilometer Array [32], and the required simulations also multiply by many folds, which is exhaustive for present compute-intensive Monte Carlo frameworks. MGMR3D, thus, opens up the novel opportunity of making such multiparameter study plausible by producing large simulation sets with very little compute resources. A detailed study along these lines will be investigated in a follow-up work.

As a final proof of the proposed procedure we have used MGMR3D to extract X_{max} from LOFAR data that have been used in earlier studies. An average X_{max} resolution of 21 g/cm^2 is found which is competitive to the average resolution of 14.5 g/cm^2 obtained using the CoREAS based method. It is also shown that an energy resolution of 19% can be reached with MGMR3D.

In conclusion, our findings show that the latest version of MGMR3D, for specific geometries discussed in this paper, can be used as a fast and efficient tool to reconstruct shower parameters, and for high-precision studies, it can be combined with Monte Carlo simulations as a preliminary estimator to help reduce the required simulation landscape and expedite the analysis.

ACKNOWLEDGMENTS

APPENDIX A: EXAMPLE FROM LOFAR DATA

A comparison of the radio profiles between CoREAS and MGMR3D for one measured shower is shown in
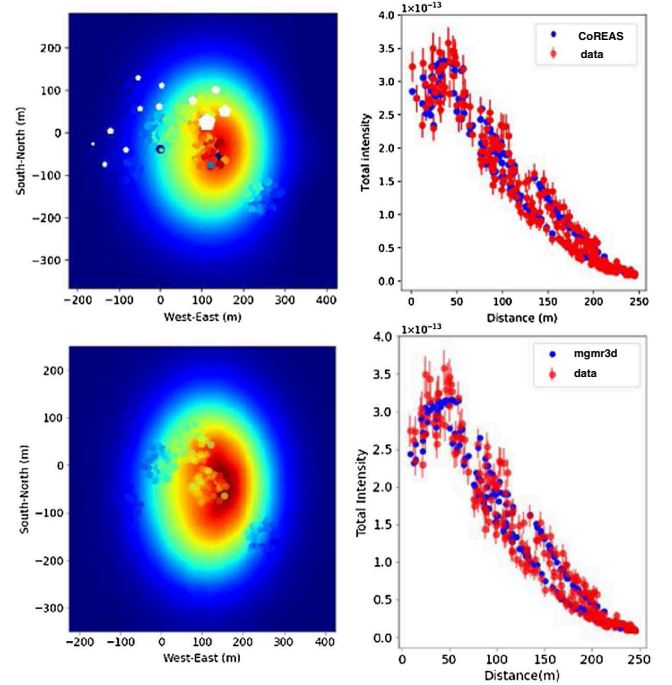

FIG. 14. Example of a measured shower fitted with CoREAS (top panel) and MGMR3D (bottom). Top panel, left: antenna configuration on the ground with color coded intensity with the best-fitting simulated footprint with CoREAS on the background. The one-dimensional LDF intensity profile for CoREAS (right). This figure is adapted from LOFAR reconstruction library catalogs, and also features the particle detectors shown by the white hexagons. Bottom panel, left and right: similar to the panel above but here simulations are done with MGMR3D. For reconstructed shower parameters see Table III.

TABLE III.   Table parameters for showers shown in Fig. 14. The core position is given as [east, north](m) with respect to the center of the Superterp.

	No.	X_{max} [g/cm^2]	Reduced χ^2	Core position [E, N] (m)
CoREAS	1	679.3	1.15	[102.1, −42.0]
MGMR3D	1	675.2	1.25	[98.6, −55.6]

Fig. 14, and the corresponding reconstructed parameters are in Table III.

APPENDIX B: PROGRAMMING DETAILS

The latest version of the program can be downloaded from [33]. This version contains the improved parametrizations, realistic error model discussed in this paper, as well as the functionality to include antenna response functions, relevant for the application to measured data.

[1] O. Scholten, K. Werner, and F. Rusydi, Astropart. Phys. **29,** 94 (2008).

[2] G. Askaryan, Sov. Phys. JETP **14,** 441 (1962).

[3] G. Askaryan, Sov. Phys. JETP **21,** 658 (1965).

[4] S. Buitink et al., Nature (London) **531,** 70 (2016).

[5] J. Alvarez-Muniz, W. R. Carvalho, Jr., and E. Zas, Astropart. Phys. **35,** 325 (2012).

[6] T. Huege, M. Ludwig, and C. W. James, AIP Conf. Proc. **1535,** 128 (2013).

[7] K. D. de Vries, O. Scholten, and K. Werner, Astropart. Phys. **45,** 23 (2013).

[8] K. D. de Vries and O. Scholten, AIP Conf. Proc. **1535,** 133 (2013);

[9] O. Scholten, T. N. G. Trinh, K. D. de Vries, and B. M. Hare, Phys. Rev. D **97,** 023005 (2018).

[10] J. D. Jackson, Classical Electrodynamics (Wiley, New York, NY, 1999), 3rd ed., ISBN 9780471309321.

[11] D. A. Butler, Ph.D. thesis, Karlsruher Institut für Technologie (KIT), 2020, 51.03.04; LK 01.

[12] A. Zilles, O. Martineau-Huynh, K. Kotera, M. Tueros, K. de Vries, W. Carvalho, V. Niess, N. Renault-Tinacci, and V. Decoene, Astropart. Phys. **114,** 10 (2020).

[13] T. N. G. Trinh, O. Scholten, S. Buitink, K. D. de Vries, P. Mitra, T. Phong Nguyen, and D. T. Si, Phys. Rev. D **105,** 063027 (2022).

[14] K. Kamata and J. Nishimura, Prog. Theor. Phys. Suppl. **6,** 93 (1958).

[15] T. N. G. Trinh et al., Phys. Rev. D **93,** 023003 (2016).

[16] T. K. Gaisser and A. M. Hillas, in International Cosmic Ray Conference (Central Research Institute for Physics of the Hungarian Academy of Sciences, Budapest, 1977), Vol. 8, p. 353.

[17] S. Andringa, R. Conceição, and M. Pimenta, Astropart. Phys. **34,** 360 (2010).

[18] R. Conceição, S. Andringa, F. Diogo, and M. Pimenta, J. Phys. Conf. Ser. **632,** 012087 (2015).

[19] P. Mitra, Ph.D. thesis, Vrije Universiteit Brussel, 2021.

[20] P. Schellart et al., Astron. Astrophys. **560,** A98 (2013).

[21] O. Scholten et al., Phys. Rev. D **94,** 103010 (2016).

[22] J. Dennis, D. Gay, and R. Welsch, ACM Trans. Math. Softw. **7,** 367 (1981).

[23] P. Schellart et al., Astron. Astrophys. **560,** 14 (2013).

[24] S. Buitink et al., Phys. Rev. D **90** (2014).

[25] M. P. van Haarlem et al., Astron. Astrophys. **556,** A56 (2013).

[26] S. Thoudam et al., Nucl. Instrum. Methods Phys. Res., Sect. A **767,** 339 (2014).

[27] T. Bergmann, R. Engel, D. Heck, N. Kalmykov, S. Ostapchenko, T. Pierog, T. Thouw, and K. Werner, Astropart. Phys. **26,** 420 (2007).

[28] A. Corstanje et al., Phys. Rev. D **103,** 102006 (2021).

[29] A. Nelles et al., Astropart. Phys. **65,** 11 (2015).

[30] K. Mulrey et al., J. Cosmol. Astropart. Phys. 11 (2020) 017.

[31] S. Buitink et al., Proc. Sci. ICRC2021 (**2021**) 415.

[32] A. Corstanje et al., Proc. Sci. ARENA2022 (**2023**) 024.

[33] O. Scholten, MGMR3D (2023), 10.5281/zenodo.7698097.